

# Momentum distributions and reaction mechanisms for breakup of two–neutron halos

E. Garrido

*Instituto de Estructura de la Materia, CSIC, Serrano 123, E-28006 Madrid, Spain*

D.V. Fedorov and A.S. Jensen

*Institute of Physics and Astronomy, Aarhus University, DK-8000 Aarhus C, Denmark*

---

## Abstract

A theoretical model able to describe fragmentation reactions of three–body halo nuclei on different targets, from light to heavy, is used to compute neutron and core momentum distributions. Both Coulomb and nuclear interactions are simultaneously included. We specify the different reaction mechanisms related to various processes. The method is applied to fragmentation of  ${}^6\text{He}$  and  ${}^{11}\text{Li}$  on C and Pb. We find good agreement with the available experimental results.

---

*PACS:* 25.60.-t, 25.10.+s, 25.60.Gc

**0.0.0.1 Introduction.** Fragmentation reactions are one of the most powerful tools to investigate halo nuclei [1–4]. Not only the large interaction cross sections, but also the narrow momentum distributions of the fragments, are clear evidence of the unusual large spatial extension of such nuclei [5–8]. Their main properties are successfully described by few–body models, where the halo nucleus is viewed as an inert core surrounded by a few weakly bound nucleons [9,10]. Models for one-neutron halo breakup reactions and the corresponding momentum distributions have been discussed [11,12], but two-neutron halos clearly require different methods. Several were developed in order to understand the available experimental cross sections and momentum distributions [5–8]. These theoretical investigations fall in two independent groups. One discusses nuclear breakup reactions and applies therefore only to light targets [10,13] whereas the other focuses on heavy targets and considers only Coulomb dissociation [14–17]. At best Coulomb and nuclear breakup are computed in independent models and the cross sections subsequently simply added [18,19].

A consistent model describing two-neutron halo fragmentation on any target, from very light to very heavy, with simultaneous treatment of nuclear and Coulomb interactions was recently presented [20,21]. Absolute values are computed of all possible dissociation cross sections distinguished according to the particles left in the final state. The two-neutron removal cross sections, core breakup cross sections and interaction cross sections for different targets are in good agreement with the measurements for energies above 100 MeV/nucleon. This is the only model for breakup of two-neutron halos which uses the same two-body interactions in initial and final states, is applicable for light, intermediate and heavy targets, and provides all possible three-body observables. Even absolute cross sections are calculated successfully [20,21] considering the difficulties related to the intrinsic structures of core and target. The precision in relative quantities like momentum distributions is much higher.

The breakup reaction mechanism is inevitably different for light and heavy targets and it is therefore surprising that the momentum distributions are rather similar [6]. To understand this almost forgotten problem requires simultaneous inclusion of both Coulomb and nuclear interactions which in itself is a problem of general interest. Differential cross sections, i.e. momentum distributions of the fragments, must be computed. The purpose of this letter is then to extract the reaction mechanism in two-neutron halo breakup processes by providing evidence from model computations. The calculated momentum distributions are especially well suited as test observables as they depend sensitively on reaction assumptions.

The predictions vary substantially from the present participant-spectator model to different models where the reaction proceeds through intermediate two or three-body resonances or continuum states. The invariant neutron-neutron mass spectra after breakup of  ${}^6\text{He}$  and  ${}^{11}\text{Li}$  exemplify the large differences between reaction assumptions. Decay through two-body resonances clearly produce the same spectra for both halo nuclei in contrast to our model where the final state wave packet strongly depends on the initial halo wave function [22]. We do not use three-body continuum wave functions as in [17]. We apply in this letter the one-participant model using optical potentials for one halo particle-target interaction while the other interactions are treated by the black disk model.

**0.0.0.2 The model.** The breakup reaction is described as a superposition of three independent reactions, each corresponding to the interaction with the target of one of the three constituents in the halo projectile. Thus, in each of these three reactions only one of the constituents (participant) interacts with the target, while the other two are mere spectators. In the center of mass frame of the halo nucleus we obtain for a spinless target that the differential cross sections for absorption and elastic scattering of the participant ( $i$ ) by

the target (0) are given by [10]

$$\frac{d^6\sigma_{abs}^{(i)}(\mathbf{P}', \mathbf{p}'_{jk})}{d\mathbf{P}'d\mathbf{p}'_{jk}} = \sigma_{abs}^{(0i)}(p_{0i})|M_s(\mathbf{p}_{i,jk}, \mathbf{p}'_{jk})|^2 \quad (1)$$

$$\frac{d^9\sigma_{el}^{(i)}(\mathbf{P}', \mathbf{p}'_{jk}, \mathbf{q})}{d\mathbf{P}'d\mathbf{p}'_{jk}d\mathbf{q}} = P_{dis}(\mathbf{q})\frac{d^3\sigma_{el}^{(0i)}(\mathbf{p}_{0i} \rightarrow \mathbf{p}'_{0i})}{d\mathbf{q}}|M_s(\mathbf{p}_{i,jk}, \mathbf{p}'_{jk})|^2 \quad (2)$$

where  $M_s$  is the normalized overlap matrix element between the three-body projectile and the final state spectator wave functions,  $\mathbf{P}'$  is the relative momentum in the final state between center of mass of target-participant and the spectators  $j$  and  $k$ , while  $\mathbf{p}'_{jk}$ ,  $\mathbf{p}_{0i}$  and  $\mathbf{p}_{i,jk}$  are relative momenta between particles  $j$  and  $k$ , 0 and  $i$ ,  $i$  and center of mass of  $j$  and  $k$ . The momentum transfer is denoted by  $\mathbf{q}$ , and primes denote final states.

Here  $\sigma_{abs}^{(0i)}$  and  $d^3\sigma_{el}^{(0i)}/d\mathbf{p}_{0i}$  are absorption and differential elastic scattering cross sections for two-body reactions between participant and target. These cross sections contain nuclear and Coulomb contributions as well as the interference between them. To remove elastic scattering reactions of the three-body system as a whole we introduce the probability for dissociation of the three-body system  $P_{dis}(\mathbf{q}) = 1 - |\langle \Psi | e^{i\mathbf{q}\cdot\mathbf{r}_{i,jk}} | \Psi \rangle|^2$ , where  $\Psi$  denotes the three-body projectile wave function and  $\mathbf{q}_{cm} \propto \mathbf{q}$  is the momentum transfer to the center of mass of the projectile.

The observable momentum distributions for any fragment are obtained by integration of Eqs.(1) and (2) over the remaining variables [10]. When the participant is charged this integration over  $q$  diverges logarithmically for small  $q$ . The divergence disappears by removal of the virtual excitations arising at impact parameters larger than the adiabatic distance. Since the energy transfer also must be larger than the three-body separation energy a minimum momentum transfer is established, i.e.  $q > q_{min}$ , see [20]. The model then gives two qualitatively different contributions to the measured particle momentum distributions, i.e. one where the neutron (core) is scattered by the target and one where the neutron-core (neutron-neutron) system continues its motion after the instantaneous removal of the other neutron.

**0.0.0.3 Reaction geometries.** The finite extension of the projectile constituents and the target is partially destroying the simple picture described above. Simultaneous collisions with the target of more than one constituent have to be considered. In Fig. 1 we sketch the *geometries* needed to describe the reaction. The short-range target-halo interactions only act for the constituents inside the cylinder along the beam axis around the target (Figs. 1a, b and c).

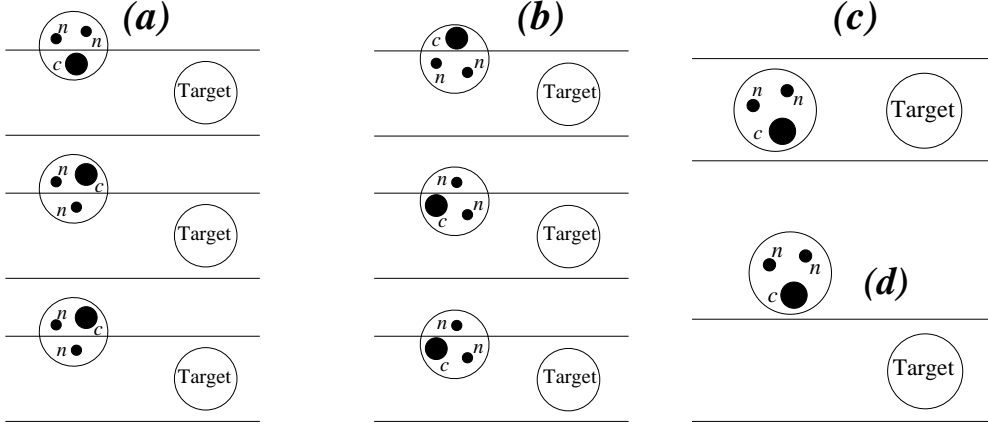


Fig. 1. Sketch of the possible geometries for the collision between target and the two-neutron plus core bound three-body projectile.

When the core is inside the cylinder the core-target interaction includes the nuclear interaction, the low impact parameter part (large momentum transfer) of the Coulomb interaction, as well as the interference between them. The reaction in Fig. 1d contains the large impact parameter part (or small momentum transfer) of the core-target interaction. It includes Coulomb elastic scattering while the two neutrons survive untouched in the final state. The value of the momentum transfer dividing into low and large impact parameters is given by [23]  $q_g = Z_0 Z_c e^2 (\gamma + 1) / (c \gamma \beta (R_0 + R_c + \pi a / 2))$ . Here  $R_0$  and  $R_c$  are charge root mean square radii of the target and the core and  $a$  is half the distance of closest core-target approach,  $eZ_0$  and  $eZ_c$  are the charges of the target and core,  $\beta = v/c$  and  $\gamma = 1/\sqrt{1 - \beta^2}$ .

Let the probabilities be  $P_c$  or  $P_n$  respectively for finding the core  $c$  or the neutron  $n$  inside the cylinders in Fig. 1. Then  $P_c = P_c^{ab} + P_c^{el}$  and  $P_n = P_n^{ab} + P_n^{el}$ , where the superscripts  $ab$  and  $el$  indicate absorption and elastic scattering by the target. When the halo projectile hits the target each of the reactions in Fig. 1a occurs with probability  $P_i(1 - P_j)(1 - P_k)$ , where the index  $i = c, n$  refers to the constituent inside the cylinder. Each reaction in Fig. 1b occurs with the probability  $P_i P_j (1 - P_k)$ , where  $i$  and  $j$  again refer to constituents inside the cylinder. In analogy the reaction in Fig. 1c occurs with the probability  $P_i P_j P_k$ . The total probability for a process producing a specific set of halo particles in the final state is now obtained by adding the probabilities of all contributing processes. Then the probabilities for two-neutron removal (core survival) and core breakup processes are:

$$P(\sigma_{-2n}) = P_c^{el} + P_n(1 - P_c) + P_n(1 - P_n)(1 - P_c), \quad (3)$$

$$P(\sigma_{-c}) = P_c^{ab}. \quad (4)$$

Two-neutron removal cross sections are correspondingly obtained as a sum

of the three contributions in Eq.(3). The first term is found by integration of Eq.(2) where the participant ( $i$ ) is the core and  $d^3\sigma_{el}^{(0i)}/d\mathbf{p}_{0i}$  the differential elastic core–target cross section containing nuclear and Coulomb interaction and the interference between them. Since  $P_c^{el}$  is the probability for the core being inside the cylinder only large momentum transfer,  $q > q_g$ , should be included in Eq.(2). However, the two–neutron removal cross section also receives a contribution from the reaction in Fig. 1d, which contains the low momentum transfer part ( $q_{\min} < q < q_g$ ) of the core–target interaction. Thus,  $q$  is actually only restricted by  $q > q_{\min}$ .

The second term in Eq.(3) corresponds to a process in which one of the halo neutrons interact with the target while the core is outside the cylinder. The contributions to the two–neutron removal cross section correspond to neutron absorption and elastic scattering obtained respectively from Eqs.(1) and (2), where the core impact parameters should be larger than the radius of the cylinder. The third term in Eq.(3) corresponds to a process in which one of the halo neutrons interact with the target while the other neutron and the core both are outside the cylinder. The contributions to the two–neutron removal cross section again correspond to neutron absorption and elastic scattering obtained respectively from Eqs.(1) and (2), where both impact parameters for the core and the other neutron should be larger than the radius of the cylinder. The core breakup cross section corresponding to Eq.(4) is simply obtained from Eq.(1) where  $\sigma_{abs}^{(0i)}$  is the core–target absorption cross section.

The neutron and core momentum distributions after two–neutron removal and core breakup reactions are the differential cross sections obtained from Eqs.(1) and (2) by leaving out the corresponding integrations [10]. They contain more details and provide therefore better tests of the reaction mechanism.

**0.0.0.4 Numerical examples.** We apply the method to fragmentation reactions of  ${}^6\text{He}$  and  ${}^{11}\text{Li}$  on carbon and lead, for which experimental neutron and core momentum distributions are available. The wave functions of the three–body halo projectiles are obtained by solving the Faddeev equations in coordinate space using the neutron–neutron and neutron–core interactions specified in [10,17]. The optical potentials for the neutron–target,  $\alpha$ –target and  ${}^9\text{Li}$ –target interactions are from [24,25], where range and diffuseness parameters for  ${}^9\text{Li}$ –target are from [26] and the energy dependence of the real part of the potential has been reduced to allow for the required large beam energy variation [20,21].

The last ingredient needed is the radius  $R_{cut}^{(s)}$  of the cylinder determining whether the spectator  $s$  is interacting with the target. We estimate  $R_{cut}^{(s)}$  by equating the experimental spectator–target absorption cross section with the absorption cross section in the black disk model  $\pi R_{cut}^{(s)2}$ . This gives  $R_{cut}^{(n)}=3.5$

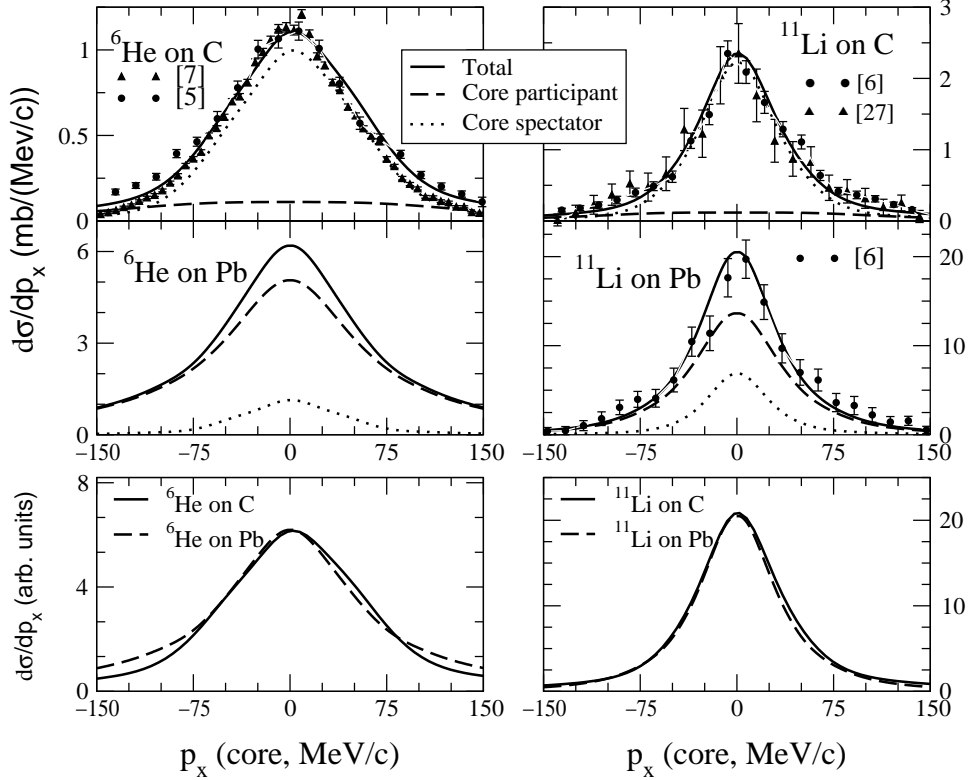


Fig. 2. Transverse core momentum distributions after fragmentation of 300 MeV/nucleon beams of  ${}^6\text{He}$  and  ${}^{11}\text{Li}$  on C and Pb. Upper part: The dashed and short-dashed lines are the contributions to the total (solid lines) from core participant and core spectator.. The experimental data are scaled to the calculations. They are for beam energies between 240 and 400 MeV/nucleon where the computed distributions are almost energy independent [10]. The data are from [5,7] for  ${}^6\text{He}$  on C, from [6,27] for  ${}^{11}\text{Li}$  on C and from [6] for  ${}^{11}\text{Li}$  on Pb. Lower part: The distributions for  ${}^6\text{He}$  on C and Pb (left) and for  ${}^{11}\text{Li}$  on C and Pb (right).

fm and 7.4 fm,  $R_{cut}^{(4\text{He})}=4.0$  fm and 7.6 fm and  $R_{cut}^{(9\text{Li})}=4.8$  fm and 7.9 fm, where the first and second numbers refer to C and Pb targets. These values are very close to those of [20,21] and the momentum distributions are in any case rather insensitive to these parameters.

The integrations of Eqs.(1) and (2) corresponding to the second contribution in Eq.(3) should only include core impact parameters larger than  $R_{cut}^{(c)}$ . This is in practice approximated by including only the part of the projectile wave function where the distance between the participant neutron and the spectator core is larger than  $R_{cut}^{(c)}$ . Analogously the integrals corresponding to the third term of Eq.(3) only include the part of the three-body wave function where the distances between the participant neutron and the spectators, neutron and core, are larger than  $R_{cut}^{(n)}$  and  $R_{cut}^{(c)}$ , respectively.

In Fig. 2 we show core momentum distributions after fragmentation of  ${}^6\text{He}$  and

$^{11}\text{Li}$  on C and Pb. Longitudinal and transverse distributions are distinguishable but very similar [10,28]. For heavy targets the main contribution comes from the core participant and the Coulomb interaction between core and target is all-decisive. The dominant reaction is that of Fig. 1d. For light targets the situation is the opposite and the core spectator contribution dominates. The core–target interaction plays a minor role and the dominant reactions are those of Figs. 1a and b with the core as a spectator.

It is significant that even though the momentum distributions from light and heavy targets are related to projectile–target interactions of different nature (nuclear neutron–target interaction and Coulomb core–target interaction) the shape of the distributions are very similar as seen in the lower part of Fig. 2, where the distributions are scaled to the same maximum. The reason is that removal of a halo neutron by a light target essentially leaves the spectators undisturbed. The resulting momentum distribution of the core is therefore close to the initial distribution inside the projectile, except for the final neutron–core interaction, which only has a relatively small effect on the core momentum [29]. For heavy targets the main contribution comes from the low momentum transfer part of the Coulomb interaction. Thus the momentum transferred to the core in the collision is small compared to its initial momentum distribution which therefore for an entirely different reason again is left relatively unchanged. This explanation is supported by the fairly good agreement between measurements and calculations.

In Fig. 3 we show transverse neutron momentum distributions after two–neutron removal of  $^6\text{He}$  and  $^{11}\text{Li}$  on C and Pb. The longitudinal distributions are hardly distinguishable from the ones shown in the figure. For light targets the core spectator contribution is again dominating, while for heavy targets the main contribution comes from processes where the core participates. The agreement with experiments is excellent for the carbon target. The computed curve is above the experimental distribution in the tails due to an experimental neutron acceptance of 50 MeV/c in both horizontal and vertical directions.

For a lead target, although experimental neutron distributions are not available, a discrepancy between computations and experiments is expected. The reason is that the neutrons, unlike the core, are highly influenced by the final state interaction between fragments [29]. In our calculations the final state interaction is properly included between the two spectator constituents as appropriate when one neutron is absorbed. On the other hand when the low momentum transfer contribution dominates (Fig. 1d) with the core as participant, as for heavy targets, the included final state interaction between the two neutrons is insufficient to describe the data. The final state interaction between all three halo constituents should be included and in particular the neutron–core interaction. This implies use of correct three–body continuum wave functions as the final state. It is in this context worth emphasizing that

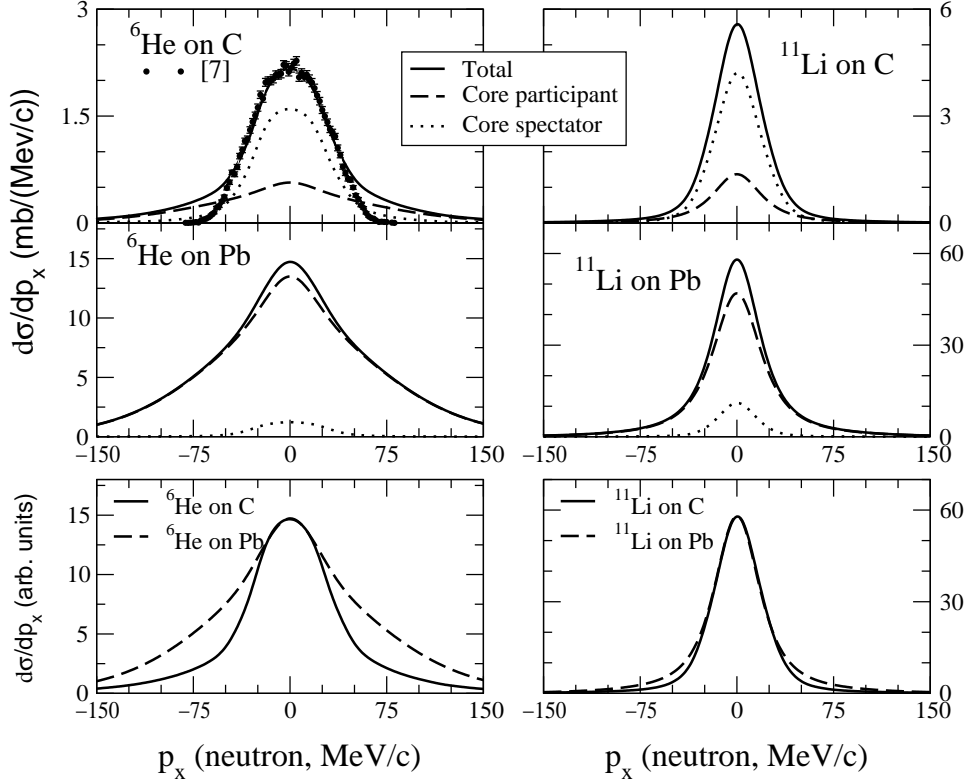


Fig. 3. The same as Fig. 2 for transverse neutron momentum distributions. Experimental data are from [7] for  ${}^6\text{He}$  on C.

such a final state would be wrong for other reaction mechanisms responsible for processes like neutron absorption.

The neutron momentum distributions for  ${}^{11}\text{Li}$  on C and Pb targets are very similar in the computation in contrast to the case of  ${}^6\text{He}$  as a projectile, see the lower part of Fig. 3. This is an interesting coincidence. For the lead and carbon targets we include respectively the neutron–neutron and neutron– ${}^9\text{Li}$  final state interaction in the dominating contributions. In both cases a low lying virtual s–state at an energy of around 100 keV is present. Since the neutron– ${}^4\text{He}$  interaction does not have such a low lying s–state the neutron momentum distributions for  ${}^4\text{He}$  on C and Pb targets differ substantially. For lead the core is the participant and for carbon the neutron is the participant. The reaction mechanisms are completely different yet the distributions are similar when the final state interactions are similar. This is a powerful illustration of the importance of the final state interaction.

**0.0.0.5 Summary and conclusions** Fragmentation reactions of two–neutron halo nuclei are described as superposition of all possible reactions where one, two or three halo constituents interact with the target. Nuclear and Coulomb interactions are simultaneously considered allowing light and



heavy targets. The two-neutron removal and core breakup cross sections can be described through processes where only one of the halo constituents interact with the target. The appropriate interactions are described by an optical potential that takes into account both elastic scattering and absorption by the target. Initial and final state interactions are identical.

Application of the method to fragmentation of  ${}^6\text{He}$  and  ${}^{11}\text{Li}$  reveals that the reactions for light or heavy targets are dominated by processes where the core is spectator or participant, respectively. For heavy targets the core-target Coulomb interaction is all-decisive. For targets of intermediate masses the Coulomb and nuclear interactions and the core spectator and participant contributions can be anticipated to compete in importance. Core momentum distributions on light and heavy targets are very similar in shape even though the reaction mechanisms are completely different. All computed neutron and core momentum distributions agree very well with the available experiments. The neutron-core interaction probably is essential for the neutron distribution for a heavy target, and the continuum three-body final state wave function is appropriate.

In conclusion the reaction mechanisms described in our fully consistent model are able to reproduce experimental total two-neutron removal and interaction cross sections [20,21] as well as core and neutron momentum distributions for two-neutron halos colliding with light and heavy targets.

**Acknowledgement.** We thank K. Riisager for continuous discussions and suggestions.

## References

- [1] K. Riisager, *Rev. Mod. Phys.* **66**, 1105 (1994).
- [2] P.G. Hansen, A.S. Jensen and B. Jonson, *Ann. Rev. Nucl. Part. Sci.* **45**, 591 (1995).
- [3] I. Tanihata, *J. Phys.* **G22**, 157 (1996).
- [4] B. Jonson and K. Riisager, *Phil. Trans. R. Soc. Lond.* **A356**, 2063 (1998).
- [5] T. Kobayashi et al., *Nucl. Phys. A* 538 (1992) 343c.
- [6] F. Humbert et al., *Phys. Lett. B* 347 (1995) 198.
- [7] D. Aleksandrov et al., *Nucl. Phys. A* 633 (1998) 234.
- [8] T. Aumann et al., *Phys. Rev. C* 59 (1999) 1252.

- [9] M.V. Zhukov, B.V. Danilin, D.V. Fedorov, J.M. Bang, I.J. Thompson and J.S. Vaagen, Phys. Rep. 231 (1993) 151.
- [10] E. Garrido, D.V. Fedorov, A.S. Jensen, Phys. Rev. C 59 (1999) 1272.
- [11] C. Dasso, S.M. Lenzi and A. Vitturi, Nucl. Phys. **A639**, 635 (1998).
- [12] R. Shyam and I.J. Thompson, Phys. Rev. **C59**, 2645 (1999).
- [13] G.F. Bertsch, K. Hencken, H. Esbensen, Phys. Rev. C 57 (1998) 1366.
- [14] Y. Suzuki, Y. Tosaka, Nucl. Phys. A 517 (1990) 599.
- [15] C.A. Bertulani, L.F. Canto, Nucl. Phys. A 549 (1992) 163.
- [16] P. Banerjee, J.A. Tostevin, I.J. Thompson, Phys. Rev. C 58 (1998) 1337.
- [17] A. Cobis, D.V. Fedorov, A.S. Jensen, Phys. Rev. C 58 (1998) 1403.
- [18] C.A. Bertulani, L.F. Canto, M.S. Hussein, Phys. Rep. 226 (1993) 281.
- [19] F. Barranco, E. Vigezzi, R.A. Broglia, Phys. Lett. B 319 (1993) 387.
- [20] E. Garrido, D.V. Fedorov, A.S. Jensen, Phys. Lett. B 480 (2000) 32.
- [21] E. Garrido, D.V. Fedorov, A.S. Jensen, Europhys. Lett. 50 (2000) 735.
- [22] E. Garrido, D.V. Fedorov, A.S. Jensen and K. Riisager, submitted for publication.
- [23] C.A. Bertulani and G. Baur, Phys. Rep. **163** (1988) 299.
- [24] E.D. Cooper, S. Hama, B.C. Clark and R.L. Mercer, Phys. Rev. **C47** (1993) 297.
- [25] M. Nolte, H. Machner and J. Bojowald, Phys. Rev. **C36** (1987) 1312.
- [26] M. Zahar et al., Phys. Rev. **C54** (1996) 1262.
- [27] H. Geissel and W. Schwab, private communication.
- [28] E. Garrido, D.V. Fedorov and A.S. Jensen, Europhysics Lett. **43** (1998) 386.
- [29] E. Garrido, D.V. Fedorov, A.S. Jensen, Phys. Rev. C 55 (1997) 1327.